

Research Statement

Andrew Hicks

November 28, 2023

1 Introduction

My current research focuses on the modeling of liquid crystals (LCs) using the cholesteric Landau-de Gennes (LdG) model, and numerical analysis of this model. In particular, in my thesis I focus on a sub-type of LC which are known as cholesteric nematic LCs, where the molecules have a chiral structure that affects their actuation and equilibrium behavior [1, 2, 3].

The crowning achievement of my thesis is new results in the numerical analysis of this cholesteric model. Namely, I have proven certain restrictions on the time-step and mesh-size appear that are not obvious to most liquid crystal scientists. I have also created a code which computes this numerical analysis and solves the LdG, with these constraints in mind. Simulation results are presented towards the end of this statement.

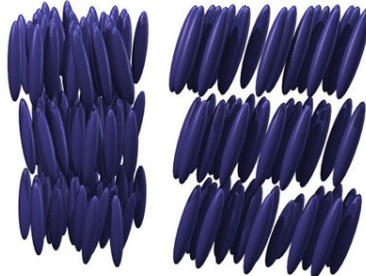


Figure 1: Liquid crystals consist of molecules that are rod-like, so they possess a general directional order (represented by the director \mathbf{n}) and an orientational order (represented by the scalar order parameter s).

2 Liquid Crystal Theory

Liquid crystals consist of rod-like molecules which allow it them to assume a state that possesses the qualities of both solids and liquids simultaneously. If we zoom into any given point in an LC, we see that the molecules there thus have a general direction in which they are pointing, as well as an orderliness to this alignment. And so the LdG theory [1, 4, 5] introduces a *tensor-valued* function Q to describe the local order (at each point in space) in the LC material. Most commonly, we have the so-called *uniaxial* state, where Q may be expressed as

$$Q = s \left(\mathbf{n} \otimes \mathbf{n} - \frac{1}{3} I \right), \quad (1)$$

where s is called the *degree-of-orientation*, and is a measure of the orientational order of the LC molecules at each point, and \mathbf{n} is called the *director*, which has unit length, $|\mathbf{n}| = 1$, and represents the average direction in which the molecules are pointing.

Let Ω be the physical domain of interest, assumed to have Lipschitz boundary Γ with outward pointing unit normal vector $\boldsymbol{\nu}$. The tensor Q belongs to the space $\mathbf{S}_0 = \{Q \mid \text{tr}(Q) = 0, Q^\dagger = Q\}$. The free energy of

the LdG model is defined as [6, 7]:

$$\begin{aligned}\mathcal{E}[Q] := & \int_{\Omega} f(Q, \nabla Q) d\mathbf{x} + \frac{1}{\eta^2} \int_{\Omega} \psi(Q) d\mathbf{x} \\ & + \frac{1}{\omega} \int_{\Gamma} g(Q) dS(\mathbf{x}) + \int_{\Gamma} \phi(Q) dS(\mathbf{x}) - \int_{\Omega} \chi(Q) d\mathbf{x},\end{aligned}\tag{2}$$

where f is the elastic function (quadratic) dependent on the material parameters ℓ_1, ℓ_2, ℓ_3 , and the twist coefficient τ_0 , which is very important to the cholesteric model, causing stripe-like patterns to emerge, which have a period of $p = 2\pi/\tau_0$ (see Figure 2). The bulk potential ψ is a quartic, double-well type of function, dependent on material parameters a_2, a_3, a_4 . The order parameter that minimizes ψ is s_0 . The surface energy, composed of the quadratic $g(Q)$ and higher-order $\phi(Q)$, accounts for *weak anchoring* of the LC (i.e. penalization of boundary conditions). This weak anchoring takes the form of *homeotropic anchoring* (where Q is penalized to have directors facing normal to the surface of Ω) and *planar degenerate anchoring* (where Q is penalized to face tangent to the surface). The function $\chi(\cdot)$ accounts for interactions with external fields. Finally, η and ω are constants resulting from the non-dimensionalization of the energy.

The strong form of this PDE, *system* defined over Ω with a tensor-valued Robin boundary condition, is as follows. In terms of indices $1 \leq i, j \leq 3$, the bulk PDE is

$$\begin{aligned}-\ell_1 Q_{ij,kk} - \ell_2 Q_{ik,kj} - \ell_3 Q_{ik,jk} - 4\ell_1 \tau_0 \varepsilon_{i\ell k} Q_{\ell j,k} \\ + \frac{1}{\eta^2} \left(-a_2 Q_{ij} - a_3 (Q^2)_{ij} + a_4 |Q|^2 Q_{ij} \right) = 0,\quad \text{in } \Omega,\end{aligned}\tag{3}$$

where only the traceless part of the tensor equation is considered. The boundary condition is given by

$$\begin{aligned}\ell_1 \nu_k Q_{ij,k} + \ell_2 \nu_j Q_{ik,k} + \ell_3 \nu_k Q_{ik,j} + 2\ell_1 \tau_0 \nu_k \varepsilon_{i\ell k} Q_{\ell j} + w_0 Q_{ij} + w_1 (Q_{ij} - Q_{ij}^\perp) \\ + \frac{1}{\omega} \left(|Q|^2 - \frac{2(s_0)^2}{3} \right) Q_{ij} = w_0 (Q_\Gamma)_{ij} - \frac{w_1 s_0}{3} (\nu \otimes \nu)_{ij},\quad \text{on } \Gamma,\end{aligned}\tag{4}$$

where, again, only the traceless part is considered.

3 Discrete Gradient Flow

We use a numerical scheme for minimizing (2) by first discretizing in time by minimizing movements [8]. Let $Q_k(x) \approx Q(x, k\delta t)$, where $\delta t > 0$ is a finite time-step, and k is the time index. Then we can minimize the energy using a sequence of elliptic problems: Given Q_k , find $Q_{k+1} \in \mathbf{V} := H^1(\Omega; \mathbf{S}_0)$ such that

$$\delta t^{-1} (Q_{k+1} - Q_k, P)_{\delta t} = -\delta_Q \mathcal{E}[Q_{k+1}; P], \quad \forall P \in \mathbf{V},\tag{5}$$

where we have defined a time-stepping inner product $(\cdot, \cdot)_{\delta t}$ by

$$(P, T)_{\delta t} := \left(\frac{1}{\eta^2} \int_{\Omega} P : T + \frac{1}{\omega} \int_{\Gamma} P : T \right).\tag{6}$$

Starting from an initial guess Q_0 , we iterate (5) until we reach a final iteration index or some other stopping criteria. In my thesis, I prove the following theorem, which gives a time-step restriction to ensure energy decrease.

Theorem 1. *The sequence $\{Q_k\}_{k=0}^{\infty}$ defined by the method above is monotonically energy decreasing, i.e.*

$$\mathcal{E}[Q_{k+1}] \leq \mathcal{E}[Q_k],$$

provided that

$$\delta t \leq 2 / \max\{a_2 + a_3^2/a_4, 2s_0^2/3\}.\tag{7}$$

It should be noted that this is not dependent on τ_0 .

4 Finite Element Method

We approximate (5) by a finite element method; in particular, we approximate Q by a finite element function $Q_h \in \mathbf{V}_h$, where \mathbf{V}_h is a finite element discretized subspace of \mathbf{V} . Using the same time-stepping procedure from before, applying it to Q_h : given $Q_{h,k}$, we find $Q_{h,k+1} \in \mathbf{V}_h$ such that

$$\delta t^{-1} (Q_{h,k+1} - Q_{h,k}, P_h)_\delta = -\delta_Q \mathcal{E}[Q_{h,k+1}; P_h], \quad \forall P_h \in \mathbf{V}_h, \quad (8)$$

We iterate this procedure until some stopping criteria is achieved. Since $\mathbf{V}_h \subset \mathbf{V}$, the same arguments in Section 3 still hold when replacing \mathbf{V} by \mathbf{V}_h . Therefore, the same time-stepping restrictions apply to the fully discrete formulation.

We seek to derive an error estimate for a local minimizer of the LdG energy. The main theoretical result for this, and indeed my most important contribution to the LC literature, is the following.

Theorem 2. *Let $Q \in \mathbf{V}$ be a local minimizer of $\mathcal{E}[\cdot]$, and let $Q_h \in \mathbf{V}_h$ be a local minimizer of $\mathcal{E}[\cdot]$. Then given the proper assumptions (such as continuity, coercivity, regularity, etc.), there exists $h_0 > 0$ and c^* such that for all $h \leq h_0$*

$$\|Q - Q_h\|_{1,\Omega} \leq c^* \inf_{P_h \in \mathbf{V}_h} \|Q - P_h\|_{1,\Omega}$$

The explicit form of h_0 is

$$h_0 = \frac{\sqrt{\alpha/(k + a'(1/\eta^2) + (2/3)(1/\omega)s_0^2)}}{2(\ell_1 + 3\ell_2 + \ell_3 + 2\sqrt{27}\tau_0 + w_0 + 3w_1 + (1/\eta^2)\bar{\Theta} + (1/\omega)\bar{\Xi})c_2c_3},$$

where

$$a' = a_2 + a_3^2/a_4,$$

and $\bar{\Theta}, \bar{\Xi}$ are constants.

This theorem is very useful; namely, it shows that higher values of τ_0 (corresponding to smaller periods of stripes in the LC structure) need a smaller mesh size to guarantee a solution sufficiently close to the true solution.

5 Numerical Simulations

Here I present the results of simulations that illustrate the cholesteric LdG model on a spherical shell for a range of twist parameters. Our software is implemented in Firedrake [9], which heavily uses the PETSc library [10]. We used Paraview [11] to visualize our simulations.

The numerical solution for Q is visualized by first performing an eigendecomposition of Q at each node of the mesh. We then set \mathbf{n} to be the eigenvector of Q corresponding to the largest eigenvalue of Q . If Q has a uniaxial form, then this choice of \mathbf{n} is consistent with (1). Finally, we compute $|\mathbf{n} \cdot \mathbf{r}|$, where \mathbf{r} is a given vector that corresponds to the computational domain, and visualize $|\mathbf{n} \cdot \mathbf{r}|$ as a scalar field.

The shell configuration is as follows. We set $\Omega = \Omega_{\text{shell},0} := \mathcal{B}(\mathbf{0}, 1) \setminus \bar{\mathcal{B}}(\mathbf{0}, 0.9)$, where $\mathcal{B}(\mathbf{0}, r)$ is an open ball of radius r . For the finite element discretization Ω_h , we set the mesh size to be $h = 0.02$. We let $\mathbf{w} = \mathbf{w}(x_1, x_2, x_3)$ be given by

$$\mathbf{w} = (\cos(\tau_0 x_3), \sin(\tau_0 x_3), 0)^\dagger. \quad (9)$$

Then, similarly to the initial conditions for the slabs, we set $\mathbf{n} = \mathbf{w}/|\mathbf{w}|$ and

$$Q_0 = s_0 (\mathbf{n} \otimes \mathbf{n} - I/3). \quad (10)$$

For $\tau_0 = 0$, we let $\mathbf{n} = \mathbf{x}/|\mathbf{x}|$, and set Q_0 as in (10).

The far left column of Figure 2 depicts the initial condition, where the color corresponds to $|\mathbf{n} \cdot \mathbf{r}|$ with $\mathbf{r} = \mathbf{x}/|\mathbf{x}|$, i.e. the radial unit vector. The stripes in the initial condition form a spiral on the spherical boundary running top to bottom, with spacing inversely proportional to τ_0 . Moreover, this figure shows the final equilibrium state of Q , corresponding to a local minimizer, for both homeotropic and planar degenerate anchoring for a range of twist values τ_0 .

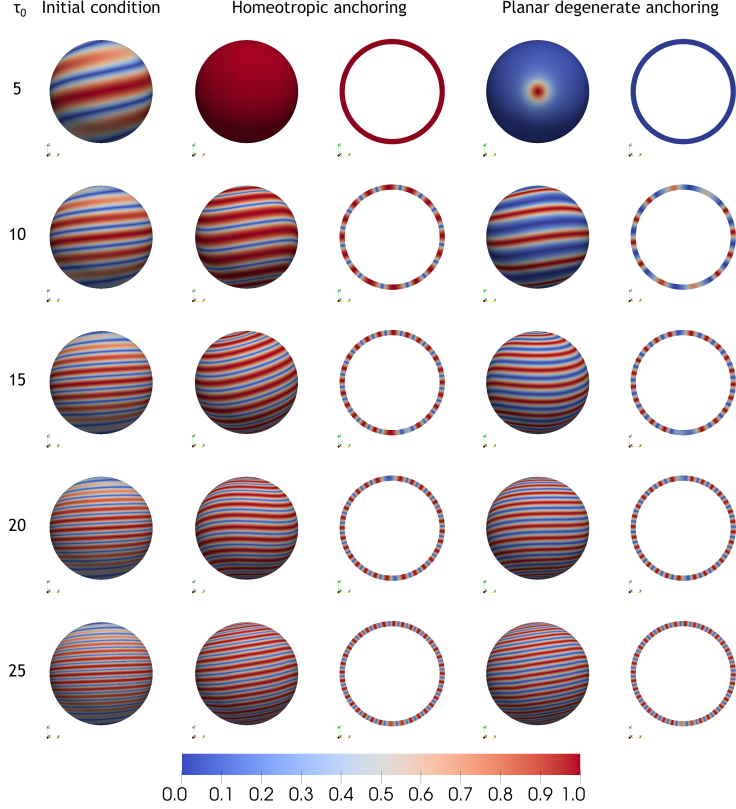


Figure 2: Centered shell ($\Omega_{\text{shell},0}$), front view. Color is proportional to $|\mathbf{n} \cdot \mathbf{r}|$ with $\mathbf{r} = \mathbf{x}/|\mathbf{x}|$. Homeotropic anchoring columns show the outer boundary and a vertical slice through the shell. Planar degenerate anchoring columns have the same format.

6 Future Work

There are several future directions which my research on the LdG model can be taken.

6.1 Optimal control problem

One of the first things that comes to mind is turning this into an optimal control problem. Following [12], the optimal control problem for the Landau-de Gennes problem may be stated as follows. Let time t vary from 0 to a specified final time, t_f . Take \mathbf{V} to be as in the previous section, and introduce the following spaces:

$$\mathcal{C} = \Omega \times (0, t_f), \quad \mathcal{G} = \Gamma \times (0, t_f).$$

We also have target functions:

$$Z_C \in L^2(\mathcal{C}), \quad Z_G \in L^2(\mathcal{G}), \quad Z_C \in H^1(\Omega).$$

The optimal control problem is to minimize the following functional:

$$\begin{aligned} J(Q, U_C, U_G) &= \frac{\beta_C}{2} \|Q - Z_C\|_{L^2(\mathcal{C})}^2 + \frac{\beta_G}{2} \|Q - Z_G\|_{L^2(\mathcal{G})}^2 + \frac{\beta_{t_f}}{2} \|Q(\cdot, t_f) - Z_{t_f}(\mathcal{C})\|_{0, \Omega}^2 \\ &\quad + \frac{\alpha_C}{2} \|U_\Omega\|_{L^2(\mathcal{C})}^2 + \frac{\alpha_G}{2} \|U_\Gamma\|_{L^2(\mathcal{G})}^2, \end{aligned} \tag{11}$$

subject to Q satisfying the strong form PDE as laid out in (3) and (4).

One notable example of an optimal control problem of this kind is the following, which we take from [12, Sec. 7.1]. We define a 2D domain with $\Omega = (0, 1) \times (0, 1)$. We set the LdG coefficients to be as they were

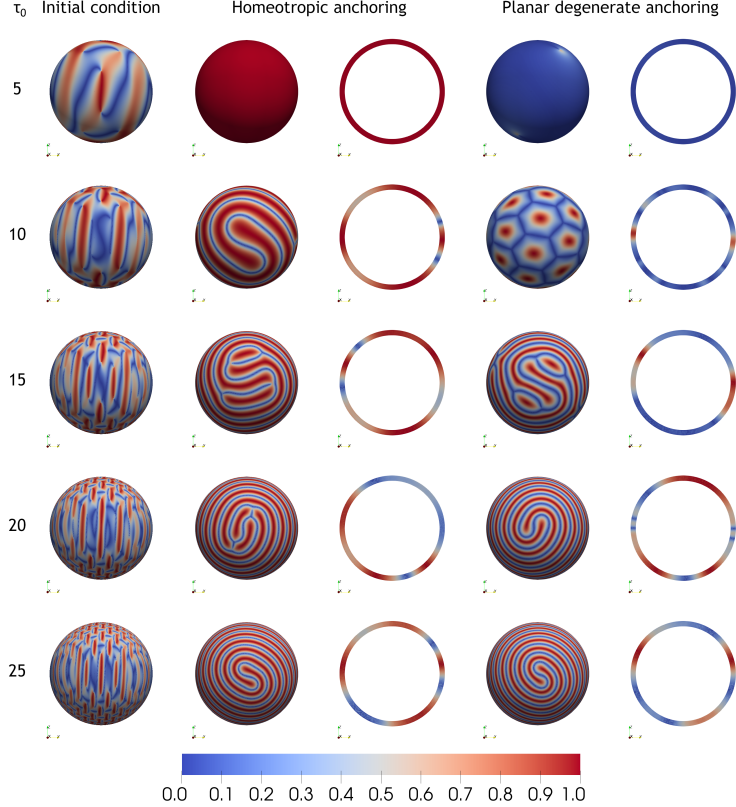


Figure 3: Centered shell: inner sphere centered at $(0, 0, 0)$, inner radius of 0.9, with oscillatory initial condition; front view.

in 5. For our initial condition, we choose \mathbf{n} such that it causes a so-called “+1/2 defect” around the center of Ω , i.e. at $(0.5, 0.5)$, and we adjust the final form $Q_0 = s_0(\mathbf{n} \otimes \mathbf{n} - I/3)$ slightly so as to insure it is both in $H^1(\Omega; \mathbf{S}_0)$ and in $C^0(\Omega; \mathbf{S}_0)$. We similarly define Z_C to be the Q -tensor based on the director that gives a +1/2 defect at the point $(0.25, 0.35)$, and $Z_G = 0$. In other words, we start with an initial condition as a defect at $(0.5, 0.5)$, and seek to find an optimal control to force it to the final state of a defect at $(0.25, 0.35)$. We will stick to an optimal control defined on the boundary and not in the bulk of Ω , so we fix $U_\Omega = 0$. The corresponding optimal control parameters are thus:

$$\beta_C = 1.0, \quad \beta_{t_f} = 1.0, \quad \alpha_C = 0.0, \quad \alpha_G = 0.01.$$

A gradient descent method is applied to solve this optimal control problem, with initial guess for the optimal control U_Γ being (once again) the Q -tensor defined as a defect at $(0.5, 0.5)$.

6.2 Experimental validation

Other future research would involve collaboration with experimentalists to validate our numerical simulation. One simulation result of interest is when we gave an oscillatory initial condition on a cholesteric shell centered at the origin. The result was a hexagonal-pentagonal tiling of the exterior of the shell. If we could replicate this experimentally, it would verify that this is not a numerical artifact, but is a true physical phenomenon. Additional measures to take numerically might involve setting an initial condition which seeks to replicate this tiling, but this may prove difficult to achieve.

Another experiment that might be verified consists of studying an offcentered shell. This shell would be defined by an outer sphere centered at the origin, and an inner sphere centered just above the origin. This would correspond to the effects of gravity pulling down the outer liquid crystal material with respect to the inner aqueous solution. Experiments have shown that, when homeotropic anchoring is applied to the

surface, a spiral forms toward the bottom that completely unwinds as one moves to the (thinner) top part of the shell. While some of our numerical experiments have proven promising in terms of reproducing similar results to this, more simulations with constants set and varying the position of the inner sphere, would prove useful in trying to replicate this pattern through an ad-hoc shape optimization.

Conclusion

In conclusion, I have made several contributions to the area of the numerical analysis of liquid crystals. I have formulated a time-stepping restriction for discrete gradient descent, stating which constants affect, and which do not, affect this. I have also given a not well-known result about the mesh size restriction dependent on certain constants, namely the twist τ_0 , showing that higher twists demand smaller mesh sizes. Finally, I have written a code that implements my numerical methods and proves their viability for simulating the cholesteric LdG model.

References

- [1] P. G. de Gennes, J. Prost, *The Physics of Liquid Crystals*, 2nd Edition, Vol. 83 of International Series of Monographs on Physics, Oxford Science Publication, Oxford, UK, 1995.
- [2] L. Tran, M. O. Lavrentovich, G. Durey, A. Darmon, M. F. Haase, N. Li, D. Lee, K. J. Stebe, R. D. Kamien, T. Lopez-Leon, Change in stripes for cholesteric shells via anchoring in moderation, *Phys. Rev. X* 7 (2017) 041029. doi:10.1103/PhysRevX.7.041029.
URL <https://link.aps.org/doi/10.1103/PhysRevX.7.041029>
- [3] M. O. Lavrentovich, L. Tran, Undulation instabilities in cholesteric liquid crystals induced by anchoring transitions, *Phys. Rev. Research* 2 (2020) 023128. doi:10.1103/PhysRevResearch.2.023128.
URL <https://link.aps.org/doi/10.1103/PhysRevResearch.2.023128>
- [4] E. G. Virga, *Variational Theories for Liquid Crystals*, 1st Edition, Vol. 8, Chapman and Hall, London, 1994.
- [5] A. M. Sonnet, E. Virga, *Dissipative Ordered Fluids: Theories for Liquid Crystals*, Springer, 2012.
- [6] H. Mori, J. Eugene C. Gartland, J. R. Kelly, P. J. Bos, Multidimensional director modeling using the Q-tensor representation in a liquid crystal cell and its application to the π -cell with patterned electrodes, *Japanese Journal of Applied Physics* 38 (1R) (1999) 135–146.
URL <http://stacks.iop.org/1347-4065/38/i=1R/a=135>
- [7] N. J. Mottram, C. J. P. Newton, Introduction to Q-tensor theory, ArXiv e-prints (Sep. 2014). arXiv: 1409.3542.
- [8] G. D. Maso, M. Forti, M. Miranda, S. A. Spagnolo, L. Ambrosio (Eds.), *Selected Papers*, Springer Collected Works in Mathematics, Ennio De Giorgi, 2006.
- [9] F. Rathgeber, D. A. Ham, L. Mitchell, M. Lange, F. Luporini, A. T. T. Mcrae, G.-T. Bercea, G. R. Markall, P. H. J. Kelly, Firedrake: Automating the finite element method by composing abstractions, *ACM Trans. Math. Softw.* 43 (3) (dec 2016). doi:10.1145/2998441.
URL <https://doi.org/10.1145/2998441>
- [10] S. Balay, S. Abhyankar, M. F. Adams, S. Benson, J. Brown, P. Brune, K. Buschelman, E. Constantinescu, L. Dalcin, A. Dener, V. Eijkhout, J. Faibussowitsch, W. D. Gropp, V. Hapla, T. Isaac, P. Jolivet, D. Karpeev, D. Kaushik, M. G. Knepley, F. Kong, S. Kruger, D. A. May, L. C. McInnes, R. T. Mills, L. Mitchell, T. Munson, J. E. Roman, K. Rupp, P. Sanan, J. Sarich, B. F. Smith, S. Zampini, H. Zhang, H. Zhang, J. Zhang, PETSc/TAO users manual, Tech. Rep. ANL-21/39 - Revision 3.19, Argonne National Laboratory (2023).

- [11] J. Ahrens, B. Geveci, C. Law, ParaView: An end-user tool for large data visualization, in: Visualization Handbook, Elesvier, 2005, ISBN 978-0123875822.
- [12] T. M. Surowiec, S. W. Walker, Optimal control of the landau–de gennes model of nematic liquid crystals, submitted (2022).